Uniform Vertical Trench Etching on Silicon with High Aspect Ratio by Metal-Assisted Chemical Etching Using Nanoporous Catalysts

ARTICLE *in* ACS APPLIED MATERIALS & INTERFACES · NOVEMBER 2013

Impact Factor: 6.72 · DOI: 10.1021/am4046519 · Source: PubMed

5 AUTHORS, INCLUDING:

Liyi Li
Georgia Institute of Technology
34 PUBLICATIONS **76** CITATIONS
SEE PROFILE

Xueying Zhao
Massachusetts Institute of Technology
9 PUBLICATIONS **27** CITATIONS
SEE PROFILE

C.P. Wong
Georgia Institute of Technology
847 PUBLICATIONS **12,775** CITATIONS
SEE PROFILE

ACS APPLIED MATERIALS & INTERFACES

Research Article

www.acsami.org

Uniform Vertical Trench Etching on Silicon with High Aspect Ratio by Metal-Assisted Chemical Etching Using Nanoporous Catalysts

Liyi Li,[†] Yan Liu,[†] Xueying Zhao,[†] Ziyin Lin,[†] and Ching-Ping Wong*[,†,‡]

[†]School of Materials Science and Engineering, Georgia Institute of Technology, 771 Ferst Drive, Atlanta, Georgia 30332, United States

[‡]Department of Electronic Engineering, The Chinese University of Hong Kong, Hong Kong

Supporting Information

ABSTRACT: Recently, metal-assisted chemical etching (MaCE) has been proposed as a promising wet-etching method for the fabrication of micro- and nanostructures on silicon with low cost. However, uniform vertical trench etching with high aspect ratio is still of great challenge for traditional MaCE. Here we report an innovated MaCE method, which combined the use of a nanoporous gold thin film as the catalyst and a hydrofluoric acid (HF)−hydrogen peroxide (H_2O_2) mixture solution with a low HF-to-H_2O_2 concentration ratio (ρ) as the etchant. The reported method successfully fabricated vertical trenches on silicon with a width down to 2 μm and an aspect ratio of 16. The geometry of the trenches was highly uniform throughout the 3D space. The vertical etching direction was favored on both (100)- and (111)-oriented silicon substrates. The reported method was also capable of producing multiple trenches on the same substrate with individually-tunable lateral geometry. An etching mechanism including a through-catalyst mass-transport process and an electropolishing-favored charge-transport process was identified by a comparative study. The novel method fundamentally solves the problems of distortion and random movement of isolated catalysts in MaCE. The results mark a breakthrough in high-quality silicon trench-etching technology with a cost of more than 2 orders of magnitude lower than that of the currently available methods.

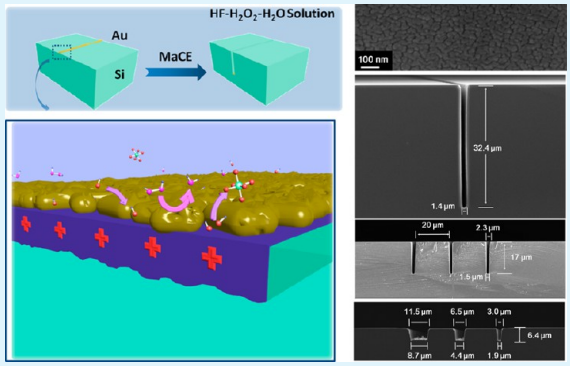

KEYWORDS: *metal-assisted chemical etching, deep trenches, high aspect ratio, uniformity, nanoporous catalyst, electropolishing*

1. INTRODUCTION

The fabrication of high-aspect-ratio vertical trenches on a silicon (Si) substrate is one of the key steps in the process flow for microelectromechanical systems,[1,2] memory devices,[3] photonic devices,[4] sensors,[5] etc. Until now, reactive ion etching (RIE)[6] and its derived technologies[7,8] have been the major methods for trench fabrication. However, their vast application in industry is hindered by the high cost of instrumentation. On the other hand, deep trenches can be fabricated by wet-etching methods as low-cost alternatives, which include basic chemical etching[9] and acidic electrochemical etching.[10−12] However, basic etching can only fabricate a vertical trench on (110)-oriented Si substrates; in acidic electrochemical etching, because the whole sample is subjected to the same environment, trenches with different geometries are difficult to integrate on the same substrate. In this sense, it is highly desirable that a novel etching method is developed to overcome the limitations of both traditional dry etching and wet etching.

In the past decade, metal-assisted chemical etching (MaCE) has been proposed as an attractive wet-etching method for the fabrication of micro-[13] and nanostructures[14−20] on Si with low cost. In MaCE, a layer of noble metal as the catalyst is deposited on the Si substrate. Etching occurs when metal-loaded Si is immersed in an etchant solution containing oxidants (mostly hydrogen peroxide, H_2O_2) and hydrofluoric acid (HF). The oxidant is catalytically reduced on the metal surface, and holes (h^+) are generated (eq 1). The holes induce dissolution of the volume of Si, surrounding the catalyst with HF coexisting in the etchant (eq 2):

$$H_2O_2 + 2H^+ \xrightarrow{\text{noble metal}} 2H_2O + 2h^+ \quad (1)$$

$$Si + 4h^+ + 6HF \rightarrow SiF_6^{2-} + 6H^+ \quad (2)$$

Subsequently, the catalyst moves into the etched space and assists further etching. From a view of the mechanism, the process of MaCE can be divided into two parts: the mass-transport (MT) and charge-transport (CT) processes. MT includes the transport of reactants (HF and H_2O_2) and products (H_2O and H_2SiF_6), while CT consists of the generation, transport, and consumption of h^+. In the experiment, MT can be tuned by the geometry of catalyst, while CT can be tuned by the concentration of HF and H_2O_2. The final etching profile is synergistically influenced by MT and CT. For

Received: October 21, 2013
Accepted: November 21, 2013
Published: November 21, 2013

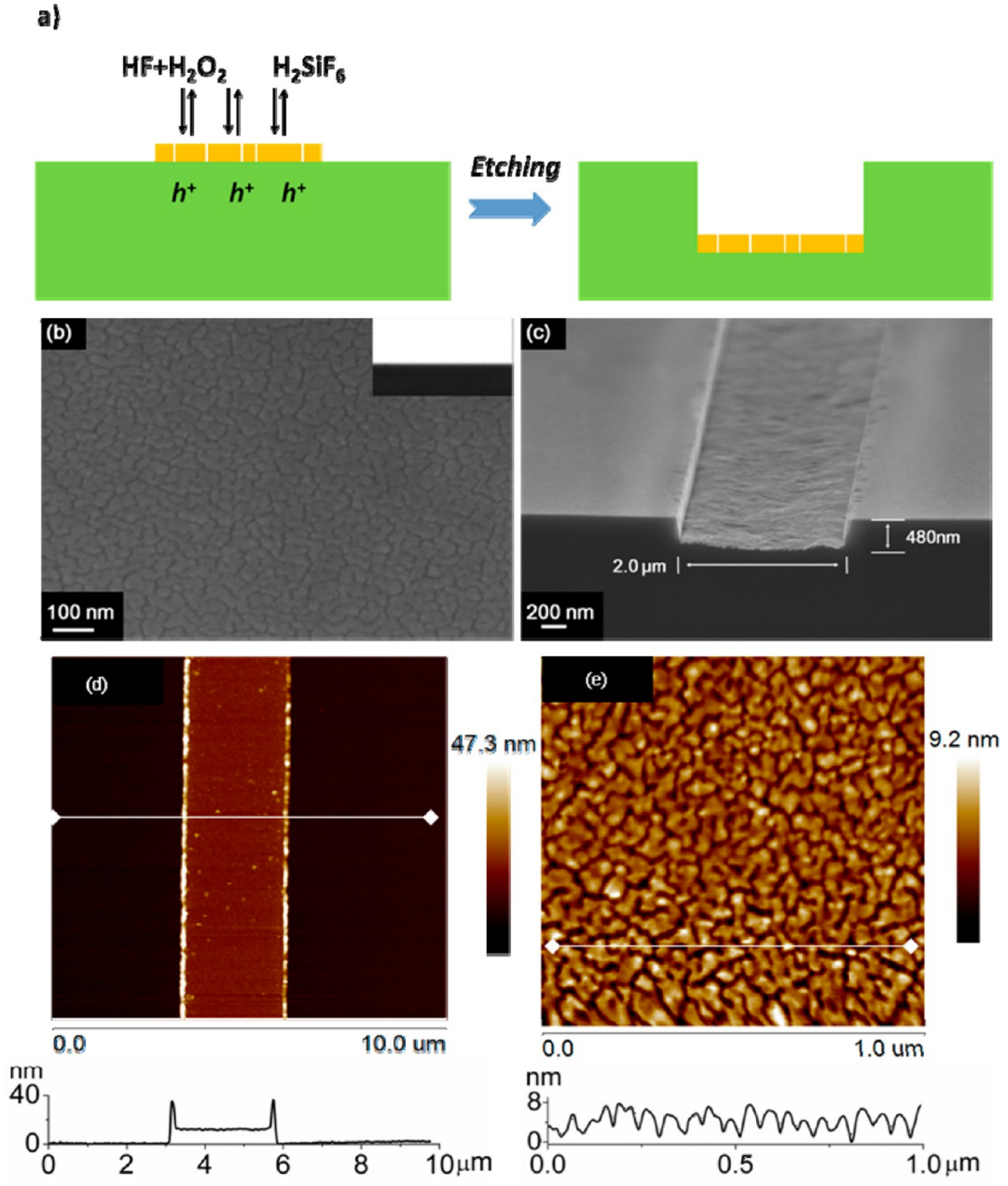

Figure 1. (a) Schematic mechanism of a through-catalyst MT process. (b) Bird's eye view SEM images of a SiO-10 nm catalyst. The inset shows the contact angle image of a water droplet on the Si−O surface. (c) Cross-sectional SEM image of the trench etched by the SiO-10 nm catalyst shown in part b for 1 min in a $\rho(0.37)^{1.8}$ etchant. (d) Overall and (e) detailed AFM height sensor image (up) and cross-sectional diagram (bottom) of the SiO-10 nm catalyst. Note: For AFM measurement, the Au stripes are patterned as an array using the standard photolithography process described in the experimental session. The overall thickness is measured after lift-off of the photoresist. Because the adhesion between Au and the Si−O surface is not strong enough to survive the lift-off process, the AFM image is collected from the remaining Au stripe. Here we assume the measured morphology and absolute thickness are identical with the Au stripes patterned by EBL because the same substrate and deposition condition are used.

convenience of the following discussion, here we define $\rho = [HF]/([HF] + [H_2O_2])$, where $[HF]$ and $[H_2O_2]$ are the concentrations of HF and H_2O_2 in moles per liter. Also, we use the format of $\rho(x)^y$ to name a specific etchant of which $\rho = x$ and $[HF] = y$.

Using large-lateral-size mesh-shaped catalysts, MaCE has successfully fabricated high-aspect-ratio wires and pillars on (100)-Si,[15] (110)-Si,[16] and even GaAs.[21] These findings inspired us to also apply MaCE to deep trench etching. In this case, isolated catalysts with small lateral sizes are required. Recently, our group has demonstrated a series of controllable nonlinear movements of isolated catalysts in MaCE, such as spiraling of a catalyst,[13,22] folding of a hinged catalyst,[23] and out-of-plane rotation of a pinned catalyst.[18,24,25] However, high-aspect-ratio vertical etching of an isolated catalyst with a uniform profile is still of great challenge. With this aspect, only shallow and irregular trenches were reported in the literature.[26] Here we identify two major factors that caused the failure: (1) The catalyst adopted continuous-film morphology. During etching, MT could hardly reach the region under the center of the catalyst. Therefore, the etching rate of this region was slower than that near the catalyst edge.[27] The uneven etch rate

dx.doi.org/10.1021/am4046519 | ACS Appl. Mater. Interfaces 2014, 6, 575−584

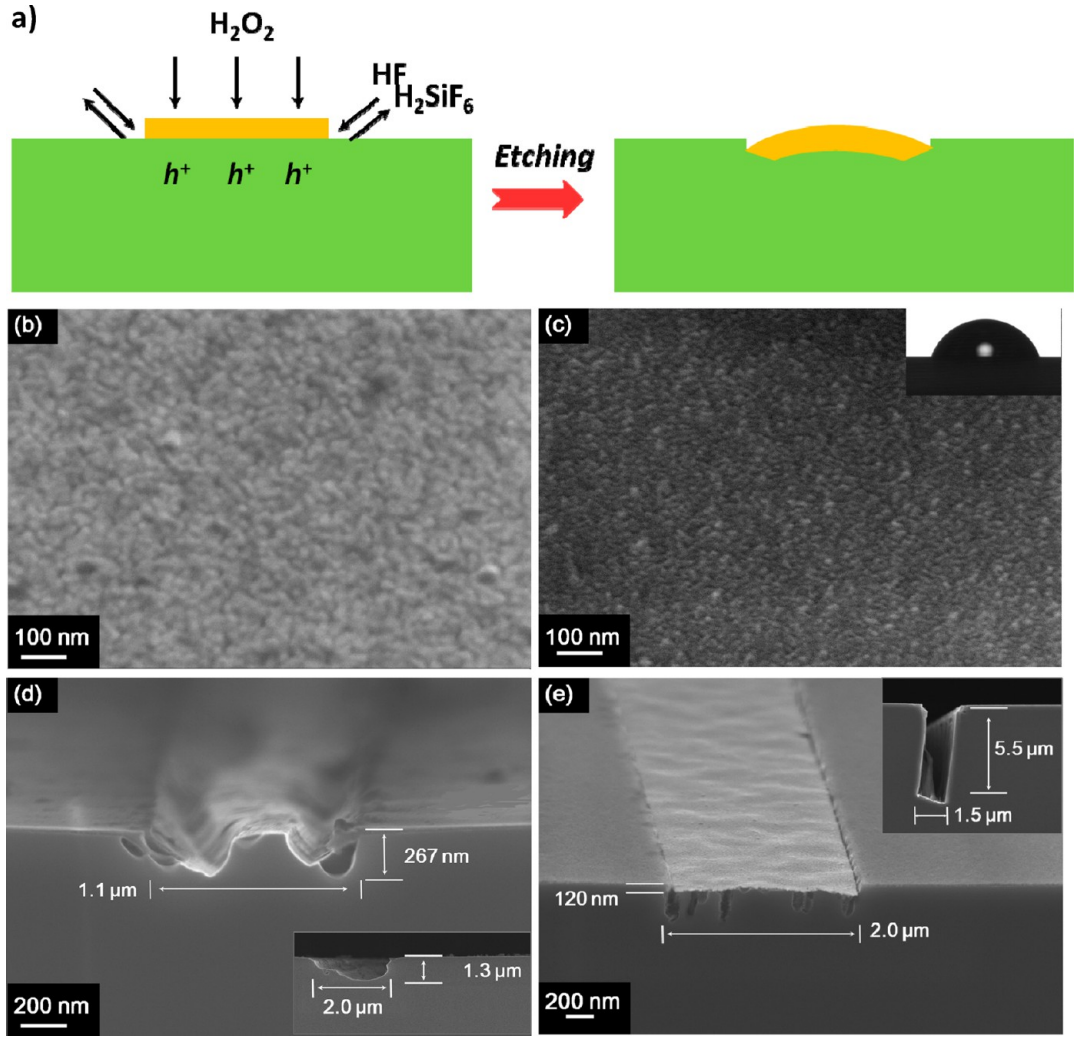

Figure 2. (a) Schematic mechanism of an edge-only MT process. Bird's eye view SEM images of (b) SiO-20 nm and (c) SiH-10 nm catalysts. Cross-sectional SEM images of the trenches etched in a $\rho(0.37)^{1.8}$ etchant for 1 min by (d) SiO-20 nm and (c) SiH-10 nm catalysts. The insets of parts d and e show the trenches etched for 10 min, with other conditions the same as those in parts d and e, respectively.

finally induced deformation of the catalyst. (2) An etchant of high ρ value (0.80−0.95) was used, in which the number of generated h^+ was less than that consumed by the process described in eq 2.[28] This condition was found to cause random movement of the catalyst.[26,29]

In this paper, we solve these issues by two fundamental innovations: (1) Gold (Au) stripes with nanoporous morphology are used as catalysts. The nanoporous morphology of Au stripes allows MT to proceed through the catalyst edge as well as the pores within the stripe (named through-catalyst MT; Figure 1a). The distance of MT is significantly shortened and evenly distributed, which guarantees a uniform high etching rate across the catalyst. We also demonstrate that the desired nanoporous Au catalyst can be facilely obtained by surface treatment of the substrate and control of the deposition thickness during electron-beam evaporation, as described in the following session: (2) The ρ value of the etchant is lowered to 37. The low-ρ etchant induced an electropolishing-favored-type (EPF) CT. Under this condition, etching is favored only along the normal of the substrate surface, which also facilitates the uniformity of the vertical etching profile.

2. RESULTS AND DISCUSSION

It has been reported that an oxygen-terminated Si surface (Si−O) dewets Au.[30] At the early stage of physical vapor deposition of a Au thin film on Si−O, separated islands of Au atoms are formed by their self-agglomeration.[31] As deposition proceeds, the islands grow and the gaps between them become narrower, before they finally coalesce into a continuous film. By control of the amount of deposited Au, i.e., its nominal thickness (referred to as thickness in the following discussion unless specified), we can obtain a partially coalesced Au film with few-nanometer-wide gaps between Au islands. On the basis of this idea, a (100)-oriented single-crystal Si substrate (referred to as Si in the following unless specified) was coated with a layer of polymer resist. A 2.00 ± 0.03-μm-wide stripe-shaped exposed area was patterned by electron-beam lithography (EBL) because of high patterning accuracy. EBL is used in the fabrication of all other patterns in this paper unless specified. After treatment with oxygen plasma, the exposed area on Si showed a water contact angle of 0° (Figure 1b, inset), evidence of Si−O surface chemistry that was primarily composed of a silanol group (Si−O−H).[32] Subsequently, Au of 10 nm thickness was deposited on Si−O (named the SiO-10 nm catalyst) by electron-beam evaporation. By scanning electron

dx.doi.org/10.1021/am4046519 | ACS Appl. Mater. Interfaces 2014, 6, 575−584

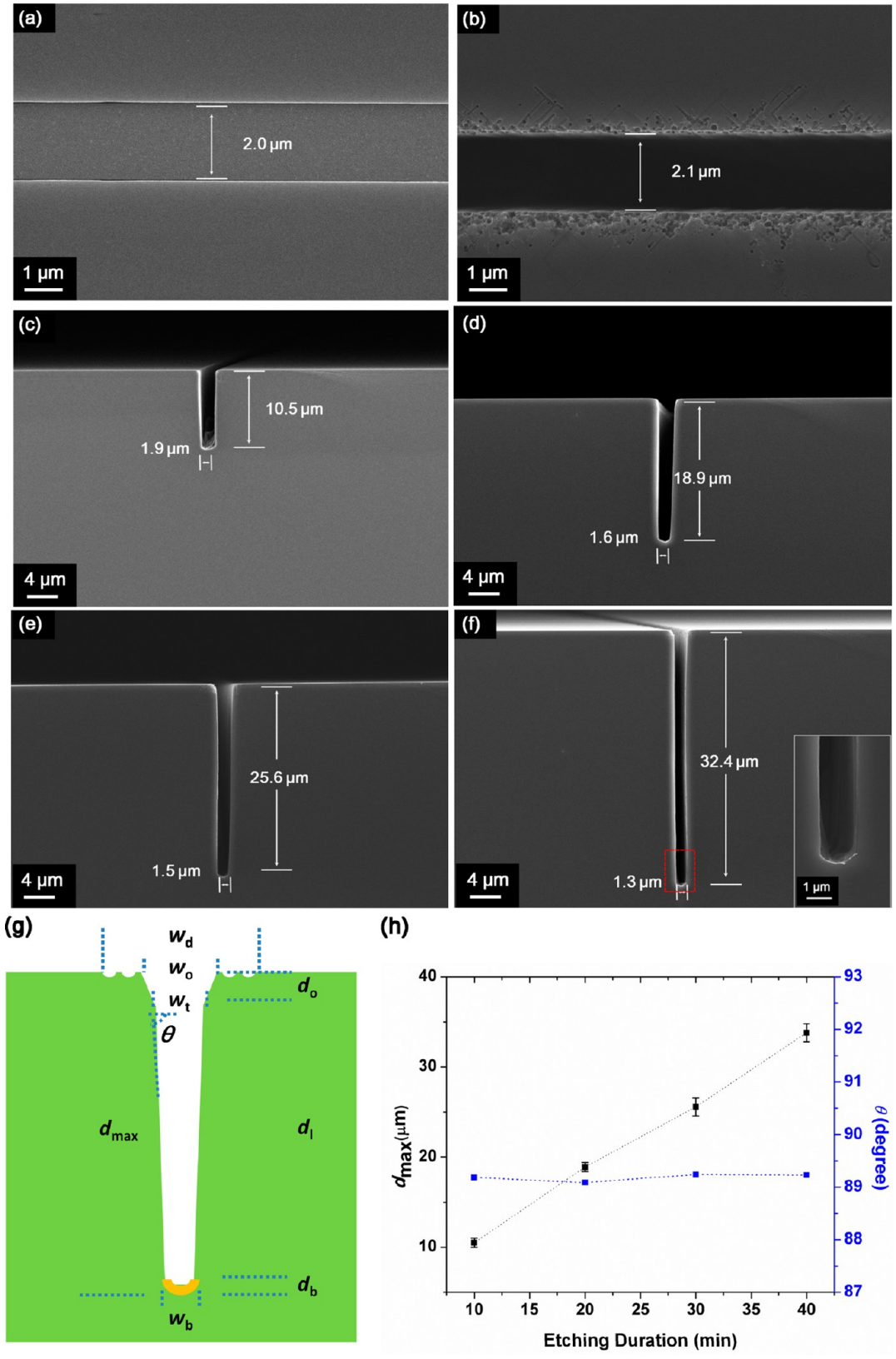

Figure 3. (a) Top view SEM image of a 2-μm-wide SiO-10 nm catalyst. (b) Top view SEM image of the trench etched by the SiO-10 nm catalyst in a $\rho(0.37)^{1.8}$ etchant for 40 min. Cross-sectional SEM images of the trench etched by the SiO-10 nm catalyst in a $\rho(0.37)^{1.8}$ etchant for (c) 10, (d) 20, (e) 30, and (f) 40 min. The inset in part f shows the magnified image of the red-circled area in part f. (g) Schematic definition of geometric parameters of the etched trench shown in parts c–f: the lateral dimensions are defined as the width of the hole diffusion region (w_d), trench opening (w_o), trench top (w_t), and trench bottom (w_d); the vertical dimensions are defined as the depth of maximum penetration (d_{max}), opening region (d_o), linear region (d_l), and bottom region (d_b) and the angle between the sidewall and Si top surface (θ). The tapering angle α is defined as the complementary angle of θ, i.e., $\alpha = 90° - \theta$. (h) Plot of d_{max} and θ of the trenches in parts c–f against the etching duration.

dx.doi.org/10.1021/am4046519 | ACS Appl. Mater. Interfaces 2014, 6, 575–584

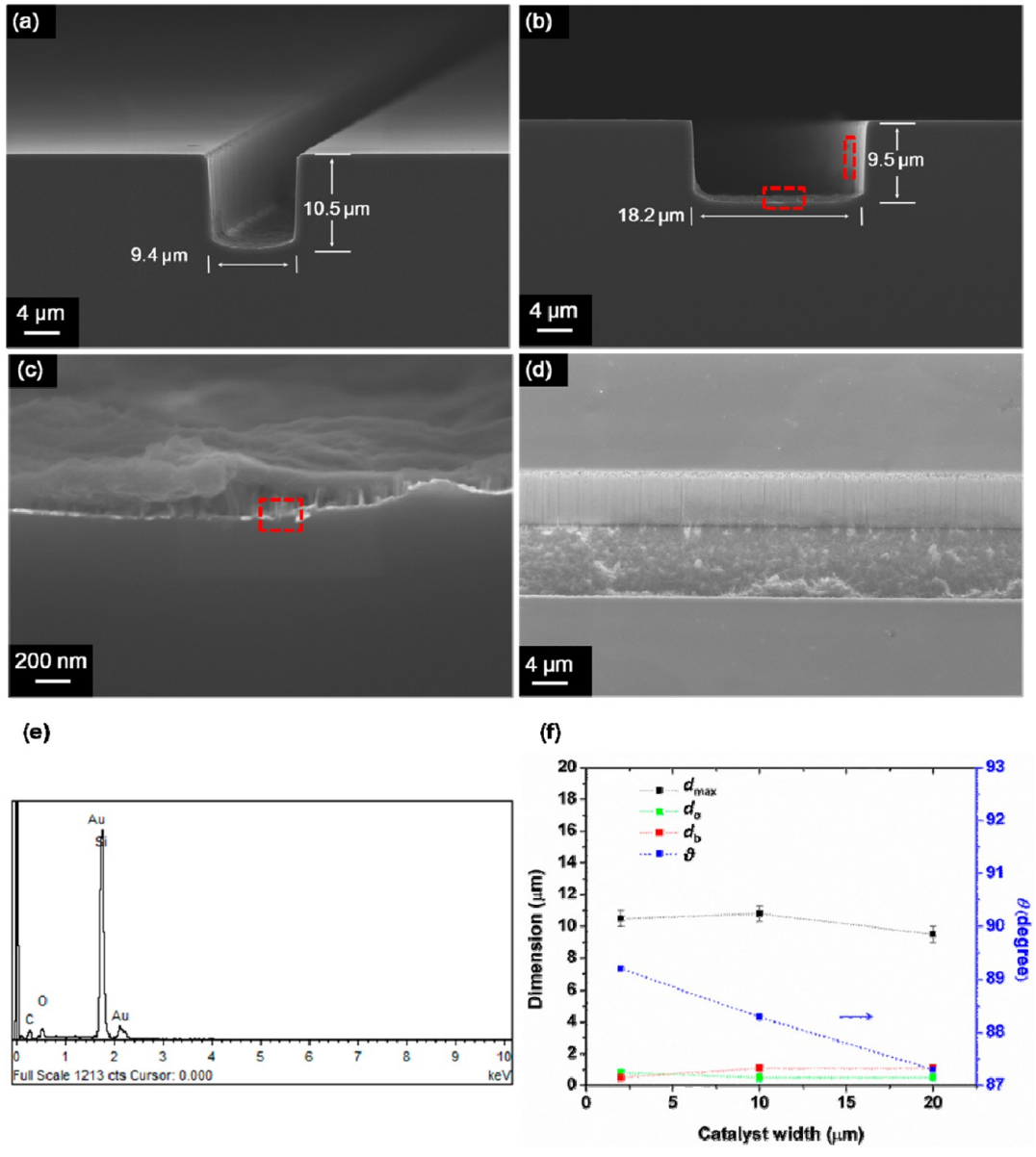

Figure 4. (a) Cross-sectional SEM images of the trenches etched in $\rho(0.37)^{1.8}$ for 10 min by the SiO-10 nm catalyst with (a) 10-μm and (b) 20-μm width. (c and d) Enlarged view of the bottom and sidewall surfaces indicated by the red-circled area in part b, respectively. (e) X-ray EDS spectrum of the bottom red-circled area in part c. The geometric parameters, d_{max} and θ, are plotted against the catalyst width.

microscopy (SEM), the nanoporous morphology within the SiO-10 nm catalyst can clearly be observed, with an average pore width of 5−10 nm (Figures 1b and S1 in the Supporting Information, SI). The Au-loaded Si was immersed in a $\rho(0.37)^{1.8}$ etchant for 1 min. (In this paper, the polymer resist was not lift-off before etching mainly because the process was found to partially remove the catalyst as well.) After etching, the SiO-10 nm catalyst moved vertically into Si by 480 nm; the sidewall of the formed trench is smooth, and the overall catalyst remains flat (Figure 1c). The nanoporous morphology of the SiO-10 nm catalyst was also characterized by atomic force microscopy (AFM) using supersharp tips. The AFM-measured thickness of the SiO-10 nm catalyst is 10.0 ± 1.0 nm (Figure 1d), identical with the maximum peak-to-valley depth of 9.8 nm within the stripe (Figure 1e). This accordance implies that the pores penetrate through the whole layer of the Au film, a necessary condition for through-catalyst MT to occur. Details of the experiments can be found in the methods part of the SI.

In contrast, if the catalysts possess continuous morphology, they are supposed to easily deform after etching because MT is only enabled from the edge of the catalyst (Figure 2a). To illustrate this point, we obtained continuous Au catalysts by increasing their thickness or treating the substrate surface with wet Au. Figure 2b shows a 20-nm-thick Au catalyst on the Si−O surface (named the SiO-20 nm catalyst); Figure 2c shows a 10-nm-thick Au catalsyt (named the SiH-10 nm catalyst) on the hydrogen-terminated Si surface (Si−H). Si−H was obtained by treating Si with a HF aqueous solution. The surface chemistry of Si−H is illustrated by their water contact angle of 69° (Figure 2c, inset).[32] Because Si−H wets Au well, Au tends to spread over the surface and coalesce into a continuous film rather than form islands like that on Si−O with the same thickness. Indeed, nanopores were hardly observed on the surfaces of SiO-20 nm and SiH-10 nm catalysts in Figure 2b,c. After 1 min of etching in the $\rho(0.37)^{1.8}$ etchant, the 20-nm-thick catalyst was seriously wrinkled. The volume of Si near the

dx.doi.org/10.1021/am4046519 | ACS Appl. Mater. Interfaces 2014, 6, 575−584

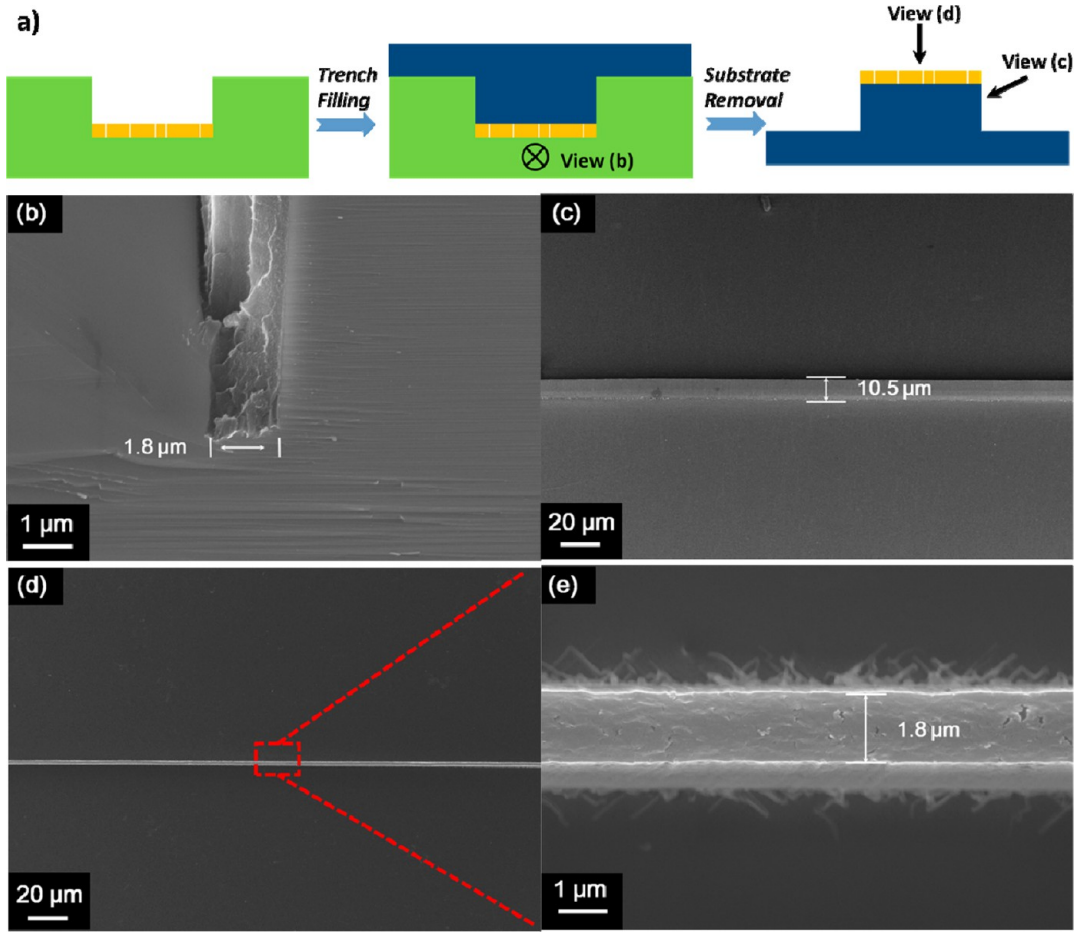

Figure 5. (a) Schematic fabrication process and observation direction of the trench replica. The green, blue, and golden blocks refer to the Si substrate, polymer replica, and Au stripe, respectively. SEM images of (b) the bottom of the trench filled with the polymer replica, (c) the longer side surface of the polymer replica from a view of 45° to the horizontal plane, and (d) top view of the polymer replica. (e) Details of the red-circled area in part d.

edge of the stripe was etched by 282 nm, while the volume under the central part of the catalyst kept intact (Figure 2d).[26] For SiH-10 nm catalysts, rough pits in Si were found near the edge, while the overall etching depth was significantly lower than that using the SiO-10 nm catalyst (Figure 2e).

The difference between the etching profiles of the nanoporous catalyst and the continuous catalyst became more significant when the etching duration was prolonged. After 10 min of immersion in a $\rho(0.37)^{1.8}$ etchant, the trenches etched by both SiO-20 nm and SiH-10 nm randomly were tilted from the Si surface normal (insets of Figure 2d,e). In contrast, a uniform vertical trench was etched by the SiO-10 nm catalyst (Figure 3c). The vertical etching direction and the uniformity of the geometry was well preserved even after etching 20, 30, and 40 min, as shown in Figure 3d–f, respectively. From the top view, the width of the trench opening after 40 min of etching is 2.10 ± 0.50 μm (Figure 3b), slightly wider than that of the original catalyst (Figure 3a). The contours of the trenches' cross sections are schematically drawn in Figure 3g with the definition of geometric parameters. It should be noted that the SiO-10 nm Au catalyst patterned by photolithography rendered similar results (Figure S2 in the SI), except with an increased edge roughness because of the lower accuracy of photolithography. Along the normal of the substrate surface, the trench contour can be divided into three regions: a top region with a roughened surface and an enlarged tapering angle; a major linear region with vertical and smooth sidewalls in the middle; a bottom region with a bended surface. The maximum depth (d_{max}) and the sidewall angles (θ) of the trenches are plotted against the etching duration (Figure 3h). d_{max} increased linearly against the etching duration: a constant etching rate is calculated to be 0.8 μm/min. This rate is significantly higher than the value reported using continuous[13,26,27] and mesh-shaped catalysts.[33] Also, unlike the trenches fabricated by deep RIE technology,[34] the sidewall of the trench etched by MaCE was intrinsically smooth without any scalloping because no passivation step was involved during the whole etching process (Figure 3f, inset). The value of θ remained within 89–90° across the 40 min of etching, indicating the high verticality of the trenches. In addition, we also tried etching of a 2-μm-wide SiO-10 nm Ag catalyst immersed in $\rho(0.37)^{1.8}$ for 10 min. The lateral geometry of the etched trench was heavily enlarged, which is probably due to dissolution of Ag in the etchant and redeposition on the sidewall of the trenches (Figure S3 in the SI). The failure of Ag in producing a vertical trench indicates that, besides the controllability during etching, the chemical stability of the metal catalyst cannot be ignored.

In the literature, some discontinuous metal catalysts, including separated nanoparticles[35−37] and a continuous film with pores,[33] have been used to obtain a vertical etching profile. However, within the etched trenches, considerable Si remained

dx.doi.org/10.1021/am4046519 | ACS Appl. Mater. Interfaces 2014, 6, 575−584

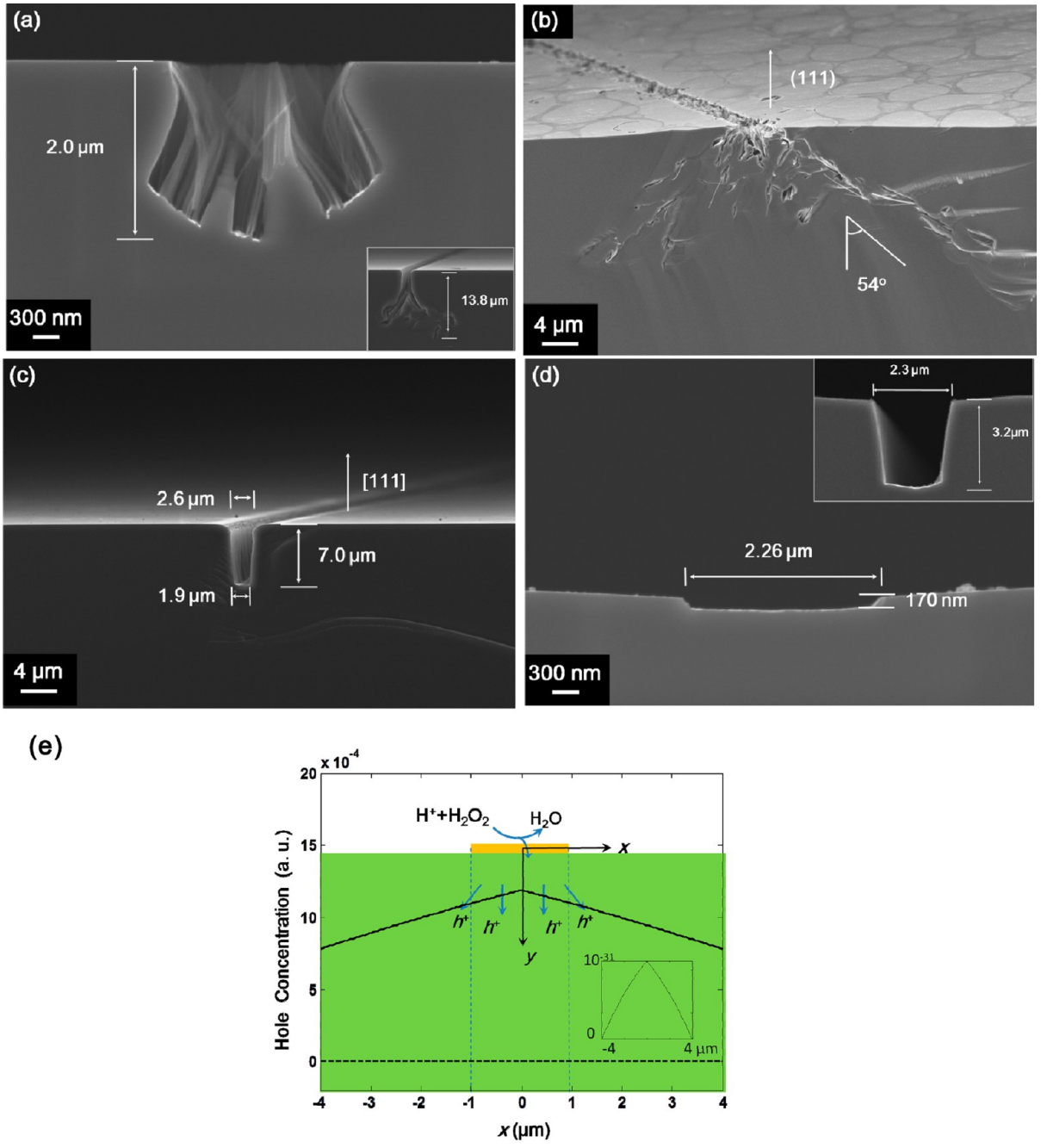

Figure 6. Cross-sectional SEM images of the trench etched by the 2-μm-wide SiO-10 nm catalyst in (a) a $\rho(0.64)^{5.4}$ etchant for 1 min, (b) a $\rho(0.64)^{5.4}$ etchant for 10 min on Si(111), (c) a $\rho(0.37)^{1.8}$ etchant for 10 min on Si(111), and (d) $\rho(0.18)^{0.9}$ for 1 min. The insets of parts a and d show the trench etched for 10 min under the same condition. (d) Modeling of the excessive hole concentration against the x axis after 1 min of etching in a 2D coordination system. The golden and green blocks refer to the Au catalyst and Si substrate. The solid (—) and dashed (----) lines correspond to etching in $\rho(0.18)^{0.9}$ and $\rho(0.37)^{1.8}$ etchants, respectively. The inset corresponds to etching in $\rho(0.37)^{1.8}$ with a smaller scale of the y axis.

not fully etched because large gaps existed between Au domains. In contrast, because the gaps in the SiO-10 nm catalyst were so narrow, Si was completely removed, as shown in Figure 3c–f. In a control experiment, we studied the etching behavior of the Au stripe with 5 nm thickness on Si–O (named the SiO-5 nm catalyst), where Au islands were found well separated by larger gaps compared to those in the SiO-10 nm catalysts (Figure S4a in the SI). After 10 min of immersion in a $\rho(0.37)^{1.8}$ etchant, a considerable amount of Si remained not fully etched (Figure S4b in the SI). The resulting etching profile appeared as bundles of Si nanowires. The above results demonstrate the unique effect of the nanoporous morphology in producing uniform vertical deep trenches with high etching rate.

To further confirm that through-catalyst MT was induced by SiO-10 nm catalysts, the etching behavior of wider Au stripes was investigated. It has been reported that if MT was limited to the catalyst edge, the etching rate would decrease as the width of the catalyst increased because of increasing difficulty of the transport of HF to Si beneath the center of the Au stripes.[27]

dx.doi.org/10.1021/am4046519 | ACS Appl. Mater. Interfaces 2014, 6, 575–584

However, as shown in Figure 4a,b, both 10-μm- and 20-μm-wide SiO-10 nm catalysts manage to penetrate a depth of ~10 μm vertically after 10 min of etching. The independence of the etching rate on the width of the catalyst supports through-catalyst MT induced by SiO-10 nm catalysts. Moreover, after etching, unlike the upward bending of the central region of the SiO-20 nm catalyst (Figure 2c), we observed a slight downward bending at the middle of the 10-μm- and 20-μm-wide SiO-10 nm catalysts (Figure 4a,b). The vertical bending distances (d_b) in the cases of 10-μm and 20-μm-wide catalysts were identical and larger than that of the 2-μm-wide catalyst case. The downward bending of the catalyst's center was probably due to a higher local hole concentration compared to the edge. Figure 4d shows a direct observation of the sidewall of the trenches, which is smooth and uniform. After 10 min of etching, both SEM observation (Figure 4c) and energy-dispersive spectroscopy (EDS; Figure 4e) confirm that the Au catalysts locate on the bottom surface of the trench, illustrating that etching is actually facilitated by the catalytic activity of the Au catalyst.

In order to prove that the trench etched by the SiO-10 nm catalyst in a $\rho(0.37)^{1.8}$ etchant was uniform throughout 3D space, an epoxy resin replica of the trench shown in Figure 3c was fabricated (Figure 5a). (Details of the filling procedure can be found in the methods part of the SI.) A representative cross-sectional SEM image (Figure 5b) shows the complete filling of the trench by resin with negligible void on the epoxy−Si interface, which means that the replica is able to provide reliable 3D geometric information of the deep trench. After curing of the epoxy resin and removal of Si, the free-standing replica was viewed from the top and side surfaces. The replica appears as a thin vertical sheet standing on a large flat plate. Across 55 μm along the sheet, the height is measured as 11.0 ± 0.5 μm (Figure 5c); the width is measured as 1.8 ± 0.3 μm (Figure 5d,e). These geometric parameters are consistent with the d_{max} and w_b value measured from cross-sectional SEM images of the trenches. The highly uniform geometry of the replica in 3D space indicates that negligible deformation of the catalyst occurred throughout the etching process.

Besides the nanoporous morphology of the Au catalyst, another important factor that contributes to the uniform vertical etching profile is the low ρ value of 0.37. Previously, etchants with high ρ value (0.60−0.96) have been used in most MaCE-related literature. As control experiments, the etching behavior of the SiO-10 nm catalyst in a $\rho(0.64)^{5.4}$ etchant was studied. Both the vertical pores and tilted branches exist in the trench after immersion in a $\rho(0.64)^{5.4}$ etchant for 1 min (Figure 6a) and 10 min (Figure 6a, inset). On the basis of the results of repeated tests, we found that the tilting angles of the branches were randomly distributed. Here we provide a tentative explanation for the coexistence of randomly aligned branches. In a high-ρ etchant where HF is relatively abundant, once holes are injected into Si, they will be consumed right away by the Si dissolution reaction (eq 2); thus, etching will favorably proceed along the direction where the fewest Si−Si bonds are required to be broken,[38] i.e., the family of ⟨100⟩ crystalline directions. In the trench shown in Figure 6a, the vertical pores probably originated from the favorable [100] direction (i.e., the vertical direction on the (100)-oriented Si substrate), while the randomly aligned branches can be related to the tendency of etching along the [010] or [001] direction. In contrast, in a $\rho(0.37)^{1.8}$ etchant, because the concentration of H_2O_2 is high, holes generated from the metal catalyst are too many to be consumed by the Si dissolution reaction (eq 2). Under this condition, a silicon oxide layer on the Si surface tends to form following distribution of the h^+ concentration. The silicon oxide layer is isotropically dissolved by HF (named EPF CT):

$$\mathrm{Si} + 4h^+ + \mathrm{H_2O} \rightarrow \mathrm{SiO}_x + \mathrm{H}^+$$
$$\mathrm{SiO}_x + \mathrm{HF} \rightarrow \mathrm{SiF_6}^{2-} + \mathrm{H}^+ + \mathrm{H_2O} \quad (3)$$

Because of the thin-film geometry of the catalyst, the region of highest h^+ concentration is located right beneath the film and so is the silicon oxide layer. In this sense, etching only prefers to proceed along the surface normal.

To further elucidate the difference between the etching profiles from $\rho(0.64)^{5.4}$ and $\rho(0.37)^{1.8}$ etchants, we studied the etching behavior of the SiO-10 nm catalyst on a (111)-oriented Si [Si(111)] substrate. As shown in Figure 6b, after 10 min of etching in $\rho(0.64)^{5.4}$, a pore is observed at an angle of 54° with the surface normal of Si(111), indicating its [100] orientation. Also, many randomly-aligned branches are observed. However, in a $\rho(0.37)^{1.8}$ etchant, only one vertical uniform trench is observed after 10 min of etching on Si(111) (Figure 6c). These results are consistent with the experiments conducted on the (100)-type Si substrate mentioned above. The results support the point that the favorable vertical-etching-direction $\rho(0.37)^{1.8}$ etchant follows the region of highest h^+ concentration rather than the crystalline orientation of the substrates, which is distinct from other wet-etching technologies.

While a high-ρ etchant deteriorates the uniformity of the vertical etching profile, the problem of excessive h^+ diffusion arises if the ρ value of the etchant is too low. In this paper, the ρ value of a $\rho(0.37)^{1.8}$ etchant is optimized so that most of h^+ are consumed by etching of Si beneath the catalyst. Only a small amount of excessive h^+ manages to diffuse away from the catalyst and induce extra etching of the top surface. From Figure 3b, a 1-μm-wide roughened area adjacent to the trench edge could be observed after 40 min of etching. The macroporous morphology of the roughened area can be related to macropore-formating CT in this region corresponding to a low concentration of diffused h^+.[12] In contrast, when a $\rho(0.18)^{0.9}$ etchant was used, the etching rate dropped to 0.2 μm/min (Figure 6d). After 10 min of etching, the overall etching rate remained at 0.3 μm/min (Figure 6d, inset). Also, on the top surface, the region near the trench edge was removed by a depth of 1 μm. The region formed by extra lateral etching expanded to a width of 5 μm with a smoothly tapered surface. The smooth surface morphology indicates that in this region excessive h^+ is so extreme that they prevail on the sidewall and top surface, which induces an electropolishing-type etching. Under the assumptions that h^+ diffuse isotropically from a constant source[27] and the catalyst moves at a constant rate, we provide a quantitative description of excessive h^+ diffusion on $\rho(0.37)^{1.8}$ and $\rho(0.18)^{0.9}$ etchants using a 2D constant source diffusion model:[26]

$$\frac{C(x,t)}{C_0} = \mathrm{erfc}\left(\frac{x}{2\sqrt{Dt}}\right)\mathrm{erfc}\left(\frac{y}{2\sqrt{Dt}}\right)$$
$$= \mathrm{erfc}\left(\frac{x}{2\sqrt{Dt}}\right)\mathrm{erfc}\left(\frac{vt}{2\sqrt{Dt}}\right) \quad (4)$$

where t, $C(x,t)$, C_0, D, and v represent the etching duration, the h^+ concentration at the x position at time t, the constant h^+ concentration on the Au surface, the nominal diffusion coefficient, and the vertical etching rate, respectively. The x

dx.doi.org/10.1021/am4046519 | ACS Appl. Mater. Interfaces 2014, 6, 575−584

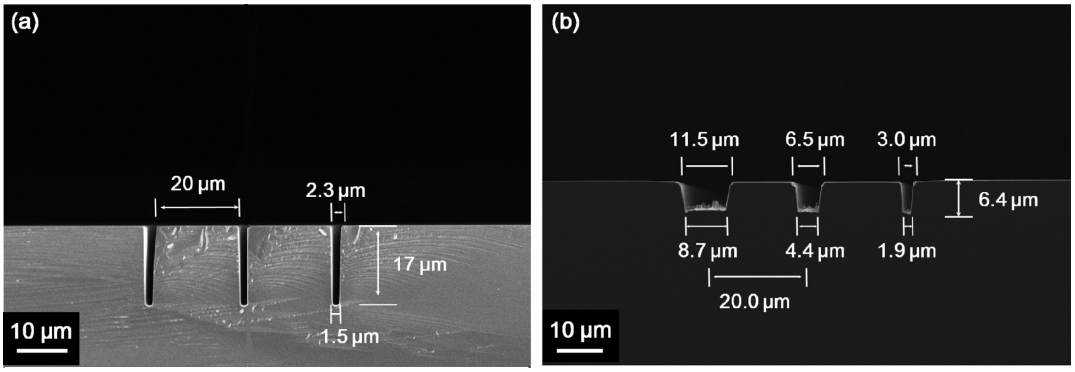

Figure 7. Cross-sectional SEM images of trenches etched in $\rho(0.37)^{1.8}$ by (a) three parallel 2-μm-wide SiO-10 nm catalysts for 20 min and (b) parallel SiO-10 nm catalysts with widths of 2, 5, and 10 μm for 10 min.

axis is defined as the direction parallel to the Si surface and normal to the catalyst; the origin point is set at the center of the catalyst before etching. The Au catalyst expands in the region of $-1 < x < 1$. D is experimentally calculated as 2.7×10^{-13} m^2/s (see the SI for details) from the data of the etching profile in a $\rho(0.18)^{0.9}$ etchant (Figure 6d) because a significant extra etching region could be observed. The same D value was used in plotting the h^+ distribution of etching in $\rho(0.37)^{1.8}$ and $\rho(0.18)^{0.9}$ etchants because the substrate and temperature were identical in both cases. Figure 6e shows the excessive h^+ concentration across the x axis after 1 min of etching. It is clear that the regions of highest h^+ concentration are located right beneath the catalyst $(-1 < x < 1)$, supporting the point in low-ρ etchant. In comparison, the amount of excessive h^+ in the $\rho(0.18)^{0.9}$ etchant is tens of magnitudes higher than that in the $\rho(0.37)^{1.8}$ etchant. The large amount of excessive holes explains the significant etching of the sidewall and top surface in the $\rho(0.18)^{0.9}$ etchant.

To demonstrate a broader range of application, multiple trenches on the same substrate were etched using the reported method. Figure 7a shows that three identical trenches were successfully etched with high aspect ratio using two parallel 2-μm-wide SiO-10 nm catalysts in a $\rho(0.37)^{1.8}$ etchant for 20 min. Their geometry highly resembles the single trench mentioned above (Figure 3d). Also, when the width of each SiO-10 nm catalyst was varied as 2, 5, and 10 μm, three trenches were etched in a $\rho(0.37)^{1.8}$ etchant with a lateral geometry variation accordingly (Figure 7b). This result proves that in MaCE the etching is catalytically induced by metal, and the etching profile can be individually tuned by the catalyst geometry on the same substrate. The capability of etching densely packed trenches with upright-standing walls as narrow as 300 nm is also demonstrated in Figure S5 in the SI.

3. CONCLUSION

In conclusion, micrometer-scale single deep trenches on Si as narrow as 2 μm with an aspect ratio up to 16 were successfully etched by using nanoporous Au stripes as the catalyst and a low-ρ HF–H_2O_2 solution. The high geometric uniformity of the etched trench throughout the 3D space was revealed by its polymer replica. By a comparative study, the vertical uniform etching behavior is attributed to the synergetic effects of through-catalyst film MT and electropolishing-favored CT. The reported method not only solves the issues of random movement of the catalyst in traditional MaCE methods but also overcomes the limitation on the crystalline orientation of substrates and the lateral geometry flexibility of the etching profile generally existing in other types of wet etchings. Because of its nature of cost orders of magnitude lower than the current major technology,[39] we believe the reported novel MaCE method has a potential a broad impact in deep trench etching application.

■ ASSOCIATED CONTENT

Supporting Information

Details of materials, instruments, experiments, and hole concentration calculation and a set of supplementary SEM images as referred to in the paper. This material is available free of charge via the Internet at http://pubs.acs.org.

■ AUTHOR INFORMATION

Corresponding Author

*Tel: (404) 894-8391. E-mail: cp.wong@mse.gatech.edu.

Author Contributions

L.L. did the experiments and wrote the manuscripts. Y.L. and Z.L. helped improve the etching condition. X.Z. did the modeling work. All authors discussed the results and revised the manuscript.

Notes

The authors declare no competing financial interest.

■ ACKNOWLEDGMENTS

The authors thank Dr. Owen Hildreth at NIST and Michael Laughter at Georgia Tech for helpful discussion. The authors thank the entire staff at IEN Georgia Tech for instrument training. The Bruker Nano Surfaces Division and David Durham are appreciated for providing the supersharp AFM tips. The authors are thankful for funding support from the National Science Foundation (NSF CMMI Grant 1130876).

■ REFERENCES

(1) Hernández, D.; Lange, D.; Trifonov, T.; Garín, M.; García, M.; Rodríguez, A.; Alcubilla, R. *Microelectron. Eng.* **2010**, *87*, 1458–1462.
(2) Ayazi, F.; Najafi, K. *J. Microelectromech. Syst.* **2000**, *9*, 288–294.
(3) Amon, J.; Kieslich, A.; Heineck, L.; Faul, T. S. J.; Luetzen, J.; Fan, C.; Huang, C. C.; Fischer, B.; Enders, G.; Kudelka, S.; Schroeder, U.; Kuesters, K. H.; Lange, G.; Alsmeier, J. *A highly manufacturable deep trench based DRAM cell layout with a planar array device in a 70nm technology*; IEEE: New York, 2004; pp 73–76.
(4) Barillaro, G.; Merlo, S.; Strambini, L. M. *IEEE J. Sel. Top. Quantum. Electron.* **2008**, *14*, 1074–1081.
(5) Henry, M. D.; Welch, C.; Scherer, A. *J. Vac. Sci. Technol., A* **2009**, *27*, 1211–1216.
(6) Bondur, J. A. *J. Vac. Sci. Technol.* **1976**, *13*, 1023–1029.

(7) Laermer, F.; Schilp, A. Method of Anisotropically Etching Silicon. U.S. Patent 5,501,893, 1996.
(8) Wu, Y.; Olynick, D. L.; Goodyear, A.; Peroz, C.; Dhuey, S.; Liang, X.; Cabrini, S. *Microelectron. Eng.* **2011**, *88*, 2785−2789.
(9) Ahn, M.; Heilmann, R. K.; Schattenburg, M. L. *J. Vac. Sci. Technol., B* **2007**, *25*, 2593−2597.
(10) Lehmann, V.; Föll, H. *J. Electrochem. Soc.* **1990**, *137*, 653−659.
(11) Lehmann, V.; Grüning, U. *Thin Solid Films* **1997**, *297*, 13−17.
(12) Föll, H.; Christophersen, M.; Carstensen, J.; Hasse, G. *Mater. Sci. Eng., R* **2002**, *39*, 93−141.
(13) Hildreth, O. J.; Fedorov, A. G.; Wong, C. P. *ACS Nano* **2012**, *6*, 10004−10012.
(14) Huang, Z.; Geyer, N.; Werner, P.; de Boor, J.; Gösele, U. *Adv. Mater.* **2011**, *23*, 285−308.
(15) Huang, Z.; Zhang, X.; Reiche, M.; Liu, L.; Lee, W.; Shimizu, T.; Senz, S.; Gösele, U. *Nano Lett.* **2008**, *8*, 3046−3051.
(16) Huang, Z.; Shimizu, T.; Senz, S.; Zhang, Z.; Zhang, X.; Lee, W.; Geyer, N.; Gösele, U. *Nano Lett.* **2009**, *9*, 2519−2525.
(17) Kim, J.; Kim, Y. H.; Choi, S.-H.; Lee, W. *ACS Nano* **2011**, *5*, 5242−5248.
(18) Rykaczewski, K.; Hildreth, O. J.; Wong, C. P.; Fedorov, A. G.; Scott, J. H. J. *Adv. Mater.* **2011**, *23*, 659−663.
(19) Xiu, Y.; Zhang, S.; Yelundur, V.; Rohatgi, A.; Hess, D. W.; Wong, C. P. *Langmuir* **2008**, *24*, 10421−10426.
(20) Liu, Y.; Xiu, Y.; Hess, D. W.; Wong, C. P. *Langmuir* **2010**, *26*, 8908−8913.
(21) DeJarld, M.; Shin, J. C.; Chern, W.; Chanda, D.; Balasundaram, K.; Rogers, J. A.; Li, X. *Nano Lett.* **2011**, *11*, 5259−5263.
(22) Hildreth, O. J.; Lin, W.; Wong, C. P. *ACS Nano* **2009**, *3*, 4033−4042.
(23) Rykaczewski, K.; Hildreth, O. J.; Wong, C. P.; Fedorov, A. G.; Scott, J. H. J. *Nano Lett.* **2011**, *11*, 2369−2374.
(24) Hildreth, O. J.; Brown, D.; Wong, C. P. *Adv. Funct. Mater.* **2011**, *21*, 3119−3128.
(25) Hildreth, O. J.; Rykaczewski, K.; Fedorov, A. G.; Wong, C. P. *Nanoscale* **2013**, *5*, 961−970.
(26) Lianto, P.; Yu, S.; Wu, J.; Thompson, C. V.; Choi, W. K. *Nanoscale* **2012**, *4*, 7532−7539.
(27) Geyer, N.; Fuhrmann, B.; Huang, Z.; de Boor, J.; Leipner, H. S.; Werner, P. *J. Phys. Chem. C* **2012**, *116*, 13446−13451.
(28) Chartier, C.; Bastide, S.; Lévy-Clément, C. *Electrochim. Acta* **2008**, *53*, 5509−5516.
(29) Tsujino, K.; Matsumura, M. *Electrochim. Acta* **2007**, *53*, 28−34.
(30) Sangiorgi, R.; Muolo, M. L.; Chatain, D.; Eustathopoulos, N. *J. Am. Ceram. Soc.* **1988**, *71*, 742−748.
(31) Boero, M.; Vincent, J. K.; Inkson, J. C.; Mejias, M.; Vieu, C.; Launois, H.; Mulheran, P. A. *J. Appl. Phys.* **2000**, *87*, 7261−7265.
(32) Lehmann, V. *Electrochemistry of Silicon*; Wiley-VCH Verlag GmBH: Weinheim, Germany, 2002; p 77.
(33) Chang, S. W.; Chuang, V. P.; Boles, S. T.; Thompson, C. V. *Adv. Funct. Mater.* **2010**, *20*, 4364−4370.
(34) Chang, C.; Wang, Y.-F.; Kanamori, Y.; Shih, J.-J.; Kawai, Y.; Lee, C.-K.; Wu, K.-C.; Esashi, M. *J. Micromech. Microeng.* **2005**, *15*, 580−585.
(35) Mohammad, Z.; Saeed Delaram, F.; Mahdi, K.; Hamed, M.; Alireza, E.; Firooz, Z. *J. Micromech. Microeng.* **2013**, *23*, 055015.
(36) Hung, S. C.; Shiu, S. C.; Chao, J. J.; Lin, C. F. *J. Electrochem. Soc.* **2010**, *157*, D496−D499.
(37) Güder, F.; Yang, Y.; Küçükbayrak, U. M.; Zacharias, M. *ACS Nano* **2013**, *7*, 1583−1590.
(38) Huang, Z.; Shimizu, T.; Senz, S.; Zhang, Z.; Geyer, N.; Gösele, U. *J. Phys. Chem. C* **2010**, *114*, 10683−10690.
(39) The cost analysis is based on the informal quotation of major materials and instruments used, as well as the output capability of MaCE and DRIE.